GEM TN-93-332

Physics Efficiency and Background Reduction for GEM Level 1 Trigger Criteria

Henk Uijterwaal
Ken McFarlane
SSC Laboratory

May 28, 1993

Abstract:

The physics efficiency and background reduction for the Level 1 trigger criteria presented in GEM TN-93-294 [1] has been determined. The event sample included physics (Higgs, heavy flavor and supersymmetry) events, events interesting for calibration purposes and minimum bias background events. Pile-up noise and multiple interactions in a bunch-crossing were included in the simulation.

After optimizing the thresholds, the physics performance for almost every physics process is close to or above the 90% level. This is roughly what one expects from a Level 1 trigger. The trigger criteria reduce the minimum bias background from 60 MHz to 15 kHz. This is close to the 10 kHz design goal, particularly when one takes into account the fact that the model used to generate this background can overestimate its contribution by a factor of up to 2.

The simulations were also tested with single particles or jets. The results are understood and show that the algorithms are well suited for the Level 1 trigger.

GEM TN–93–332.

Physics Efficiency and Background Reduction for GEM Level 1 Trigger Criteria.

Henk Uijterwaal *Ken McFarlane*

SSC-laboratory.
May 28, 1993.

Abstract

The physics efficiency and background reduction for the Level 1 trigger criteria presented in GEM TN-93–294 [1] has been determined. The event sample included physics (Higgs, heavy flavor and supersymmetry) events, events interesting for calibration purposes and minimum bias background events. Pile-up noise and multiple interactions in a bunch-crossing were included in the simulation.

After optimizing the thresholds, the physics performance for almost every physics process is close to or above the 90% level. This is roughly what one expects from a Level 1 trigger. The trigger criteria reduce the minimum bias background from 60 MHz to 15 kHz. This is close to the 10 kHz design goal, particularly when one takes into account the fact that the model used to generate this background can overestimate its contribution by a factor of up to 2.

The simulations were also tested with single particles or jets. The results are understood and show that the algorithms are well suited for the Level 1 trigger.

1 Introduction.

This document is a detailed write-up of the results on Level 1 triggers presented in [3] and answers some of the open questions raised there.

To understand the performance of the trigger on complete events, one first has to understand the response of the trigger system to single particles or jets. In principle, the trigger should find every particle above threshold within the detector acceptance. The trigger simulations have therefore been tested with single particles. Section 4 discusses the results.

After the behavior for single particles is understood, one can test the performance of the global trigger. The global trigger combines the output of the component triggers (the so-called *trigger primitives*) and decides to accept or reject the event. Section 5 shows the physics acceptance and background reduction for a various processes using the trigger criteria presented in [1].

The trigger thresholds suggested in [1] were preliminary and should be optimized to maximize the background reduction and physics acceptance. This is discussed in section 6.

It will be shown that backgrounds at Level 1 are well under control although there are still a number of open questions. Section 7 summarizes the results from the studies presented here and discusses how to proceed from here.

2 Event generation and detector simulation.

2.1 Event generation.

The events used to determine the background reduction and physics acceptance of the trigger were generated with PYTHIA [4] or ISAJET [5]. Table 1 gives an overview of the generated processes and the cuts used at the generator level. Details about the generator setups can be found in appendix A and B. The generated interactions include new physics (Higgs, heavy flavor production and super-symmetry), processes interesting for calibration purposes (Z^0- and $W^{\pm}$-production) and minimum bias background events.

The only kinematic constraint at the generator level was that the final state particles are within the geometrical acceptance of the detector. The trigger efficiency can then be defined as the number of events accepted by the trigger divided by the number of generated events. In order to get an impression of the effect of the more restrictive cuts used in the analysis of the events (see [2]), a second sample of $H^0 \to \gamma\gamma$ events with cuts close to the ones used in a physics analysis of this process was generated.

The events used to study the response of the trigger system to single particles were generated with the single particle gun available in the **gemgen** [6] package. p_T, η and ϕ for these particles were chosen at random in the range of interest. Single jets were created by fragmenting (using PYTHIA) a single d-quark with random p_T, η and ϕ. It should be noted that this method for generating single jets is slightly unrealistic but, at present, it is the only method available.

Process	*Generator*	M_{H^0} [GeV]	M_t	$M_{\tilde{g}}$	*Constraints.*
$H^0 \to \gamma\gamma$	PYTHIA [4]	80, 110, 140	140	–	$\lvert\eta_\gamma\rvert \leq 3.0$.
$H^0 \to \gamma\gamma$	PYTHIA	80, 110, 140	140	–	$\lvert\eta_\gamma\rvert \leq 2.5$, $p_{T,\gamma} \geq 20.0$ GeV and $\lvert\cos\Theta^*\rvert \leq 0.6$.
$H^0 \to \tau\tau$	PYTHIA	140	140	–	$\lvert\eta_\tau\rvert \leq 3.0$.
$H^0 \to Z^0Z^* \to \ell^+\ell^-\ell^+\ell^-$.	PYTHIA	140	140	–	$\ell = e, \mu$ and $10 \leq P_{T,Z^0} \leq 120$ GeV, see also [9].
$H^0 \to Z^0Z^0 \to e^+e^-\mu^+\mu^-$	ISAJET [5]	400	140	–	$50 \leq p_{T,Z^0} \leq 20000$ GeV and $\lvert\eta_{Z^0}\rvert \leq 3.0$.
$H^0 \to Z^0Z^0 \to e^+e^-$jet jet	ISAJET	800	140	–	$50 \leq p_{T,Z^0} \leq 20000$ GeV and $\lvert\eta_{Z^0}\rvert \leq 3.0$.
$H^0 \to Z^0Z^0 \to e^+e^-\nu\bar{\nu}$	ISAJET	800	140	–	$50 \leq p_{T,Z^0} \leq 20000$ GeV and $\lvert\eta_{Z^0}\rvert \leq 3.0$.
$H^0 \to Z^0Z^0 \to \mu^+\mu^-\nu\bar{\nu}$	ISAJET	800	140	–	$50 \leq p_{T,Z^0} \leq 20000$ GeV and $\lvert\eta_{Z^0}\rvert \leq 3.0$.
$t\bar{t} + H^0 \to \ell\gamma\gamma + X$	PYTHIA	80	140	–	See [10].
$t\bar{t}$-production.	PYTHIA	140	140	–	$\lvert\eta_{t,\bar{t}}\rvert \leq 3.0$ and $t, \bar{t} \to Wb$.
SUSY, $\tilde{g}\tilde{g}$-production.	ISAJET	–	140	500	$50 \leq p_{T,\tilde{g}} \leq 20000$ GeV, $\lvert\eta_{\tilde{g}}\rvert \leq 3.0$ and $\tilde{g} \to \tilde{\gamma}$ jet.
$W^\pm \to e^\pm\nu$	PYTHIA	–	–	–	$\lvert\eta_{e^\pm,\nu}\rvert \leq 2.5$.
$W^\pm \to \mu^\pm\nu$	PYTHIA	–	–	–	$\lvert\eta_{\mu^\pm,\nu}\rvert \leq 2.5$.
$Z^0 \to e^+e^-$	PYTHIA	–	–	–	$\lvert\eta_{e^\pm}\rvert \leq 2.5$.
$Z^0 \to \mu^+\mu^-$	PYTHIA	–	–	–	$\lvert\eta_{\mu^\pm}\rvert \leq 2.5$.
Minimum Bias	PYTHIA	–	140	–	

Table 1: Overview of the generator parameters used for the events studied in this note.

2.2 Detector simulation.

The detector was simulated with version II 2.03 of the `gemfast` [7] package.

To study the physics acceptance and background reduction, a setup with 3 processes was used. The first process generated the "signal" events. The second process generated minimum bias background interactions. The third process merged the signal events with the appropriate number of background interactions (see section 2.3) and then called the detector

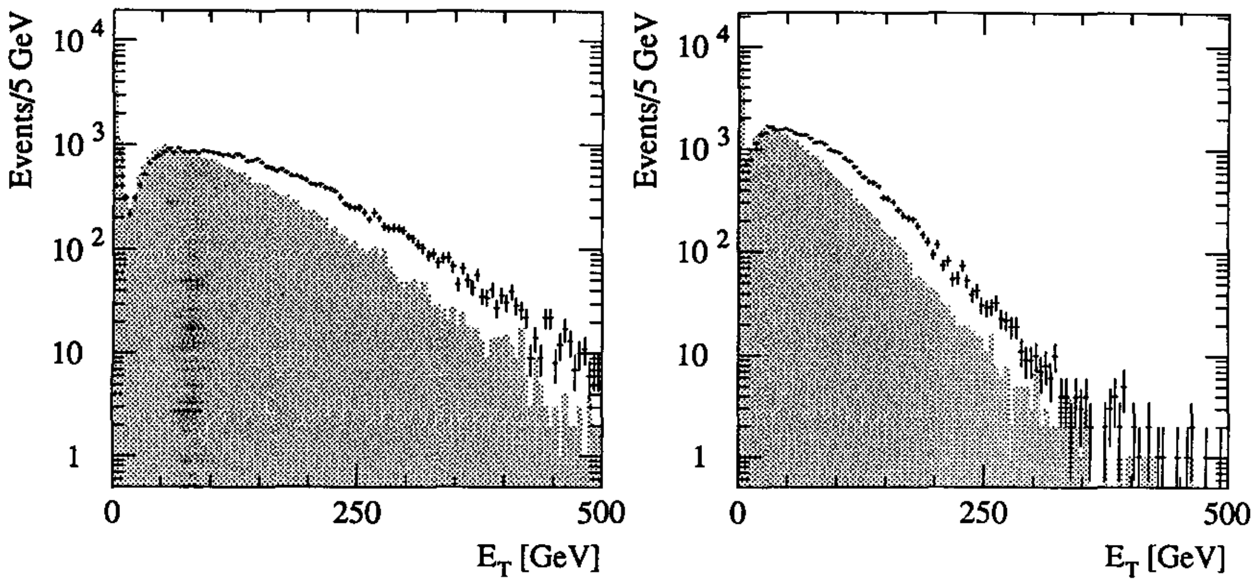

Figure 1: E_T in the forward and main calorimeter ($|\eta| \leq 6.0$, left hand side plot) and the main calorimeter only ($|\eta| \leq 3.0$, right hand side plot). The shaded area shows the distribution for an average of 1.6 events per interaction, the data points show the distribution for our model with an average of 2.6 events per interaction.

and trigger simulations. The output of the trigger simulation was written to a file and later analyzed.

When the response of the trigger system to single particles or jets was studied, the minimum bias background process was switched off and only one particle or jet was tracked through the detector.

2.3 The number of interactions in a bunch-crossing.

The number of interactions in a particular bunch-crossing depends on the luminosity and the trigger or interaction of interest. For a luminosity $\mathcal{L}$, cross-section σ and a frequency of collision f, the mean number of interactions is: $\mu = \mathcal{L}\sigma/f$. The number of interactions per crossing follows a Poisson-distribution.

For the current purpose, we take $\mathcal{L} = 10^{33}\mathrm{cm}^{-2}\mathrm{s}^{-1}$ and σ to be the inelastic cross-section for which we use the value 100 mb at 40 TeV. Elastic and diffractive scattering will not be triggered on or detected by the GEM-detector. This cross-section σ is estimated from extrapolations of accelerator data guided by cosmic ray data [8]. With a frequency of 60 MHz, we find $\mu = 1.67$ without correcting for small effects such as empty bunches. For comparison with previous calculations, we use $\mu = 1.60$.

Consider the cross-section σ to be made up of contributions from N processes (or triggers) of type i, with individual cross-sections σ_i (so that: $\sigma = \sum_{i=1}^{N} \sigma_i$). Then the probability of k

interactions in a bunch-crossing at least one of which is of type i is:

$$P(k,\sigma_i) = e^{-\mu}\,\frac{\mu^k}{k!}\left(1-(1-\frac{\sigma_i}{\sigma})^k\right) \tag{1}$$

The total probability for at least one interaction of type i in a bunch-crossing is then:

$$P(\sigma_i) = \sum_{k=1}^{\infty} P(k,\sigma_i) = 1 - e^{-\frac{\mu\sigma_i}{\sigma}} \tag{2}$$

The mean number of interactions in a bunch-crossing with at least one event of type i is:

$$\overline{n}(i) = \sum_{k=1}^{\infty} \frac{kP(k,\sigma_i)}{1-e^{-\frac{\mu\sigma_i}{\sigma}}} = \frac{\mu}{1-e^{-\frac{\mu\sigma_i}{\sigma}}}\left(1 - e^{-\frac{\mu\sigma_i}{\sigma}} + \frac{\sigma_i}{\sigma}e^{-\frac{\mu\sigma_i}{\sigma}}\right) \tag{3}$$

If $\mu\sigma_i/\sigma \ll 1$, the expected case for GEM whether σ_i represents a trigger or a physics process, we find that $\overline{n} = \mu + 1$. Or, to put it in different words, bunch-crossing containing a physics events also contains a mean of μ minimum bias background interactions. This is exactly what was generated by our detector simulation described above.

For the entire inelastic cross-section, (3) reduces to:

$$\overline{n} = \frac{\mu}{1-e^{-\mu}} \approx 2.00 \tag{4}$$

Again the number of interactions follows a Poisson distribution.

Most of the inelastic cross-section consists of minimum bias interactions and we should thus generate on average 2.0 of those interactions for each background event. However, in the simulation setup described above, we just replaced the "signal" event generator by another minimum bias generator process. As a result, the average number of minimum bias interactions per crossing is 2.6, more than what is expected.

As is shown in figure 1, the higher number of interactions correspond to a higher activity or E_T in the detector. Assuming that the probability that a background interaction is accepted by the trigger is proportional to the activity in the detector or E_T, our estimate of the background rates can be up to a factor 2 too pessimistic.

2.4 Pileup.

`Gemfast` offers two possibilities for adding off-time calorimeter pile-up noise to the simulated events: generation of uncorrelated random noise in each cell according to a Gaussian distribution and reading from a file an array that represents the summed time-weighted response from previous or later crossings for all cells. Although the latter model gives a more realistic way of modeling the effects of jets in out-of-time bunch-crossings, studies have shown that the trigger electronics can often reject these jets by determining the arrival time of the signals. Therefore, in these studies, we used the uncorrelated Gaussian pile-up noise simulation as an adequate representation of the uncorrelated residual noise.

Thermal noise was simulated according to a Gaussian distribution with the standard `gemfast` mean and RMS.

No.	Trigger	Comment
1	J_{80}	High P_T-jet.
2	(4 of J_{50})	Multi jet event.
3	E_{50}	High P_T electron or γ.
4	M_{30}	High P_T μ.
5	(2 of E_{16})	Two electrons or γ's.
6	(2 of M_{10})	Two μ's.
7	$\not{E}_{100}$	$\not{E}_T$.
8	E_{16} and $\not{E}_{50}$	Electron and $\not{E}_T$ ($W^{\pm}$, τ)
9	M_{10} and $\not{E}_{50}$	Muon and $\not{E}_T$ ($W^{\pm}$, τ)
10	J_{16} and $\not{E}_{50}$	Tau and $\not{E}_T$
11	M_{10} and (3 of J_{50})	Muon and 3 jets.
12	E_{16} and (3 of J_{50})	Electron and 3 jets.

Table 2: Suggested Level 1 trigger criteria. A logical "OR" of these criteria will accept all physics processes discussed in [1]. The trigger primitives are indicated with J_x (jet trigger), E_x (electron/γ trigger), M_x (muon trigger) and $\not{E}_x$ ($\not{E}_T$-trigger). The subscript indicates the threshold.

3 Trigger simulation.

The trigger was simulated by version 1.03 of the trigger simulation `libtrf` [11]. This version of the simulation contains simulations of the calorimeter, muon and global Level 1 triggers.

All physics efficiency studies use the algorithm for the "digital" calorimeter Level 1 trigger design described in [1]. However, as will be shown in the next section, the differences between this algorithm and the algorithm for the "analog" calorimeter Level 1 trigger design [12] for single particles are small and it is expected that resulting trigger rates and efficiencies will be the same. The algorithms will usually be referred to as the "digital" and "analog calorimeter algorithms" although the "analog" algorithm can also run on the "digital" calorimeter Level 1 trigger hardware. The muon trigger algorithm is described in [13].

The results of all component trigger simulations, the so-called trigger primitives, are used in a global Level 1 trigger routine. This routine uses the results to evaluate the trigger conditions listed in table 2. These conditions cover, see [1], all final states of the events of the GEM physics program. The routine determines the logical "OR" of the trigger conditions and accepts the event if the result is true.

The thresholds in table 2 are preliminary and will be discussed in more detail in section 6.1.

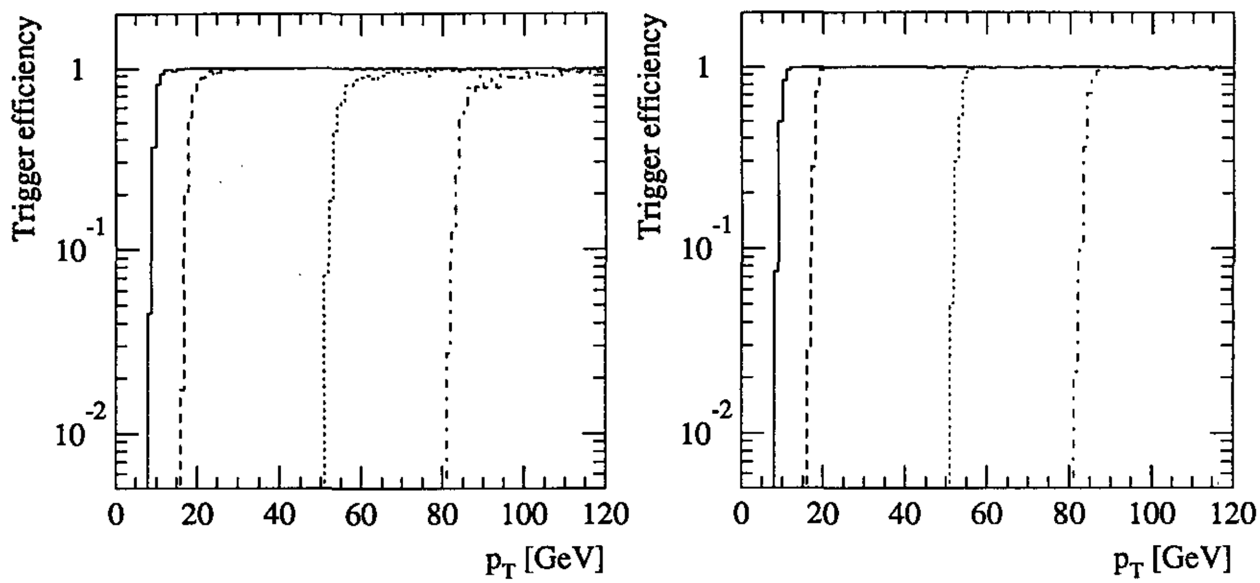

Figure 2: Trigger efficiency for electrons as a function of p_T of the electron/photon trigger, for $0.4 \leq \eta \leq 0.6$. *The left hand plot shows the probability that the digital calorimeter Level 1 algorithm finds at least 1 electron candidate above thresholds of* 8, 16, 50 *and* 80 GeV, *the right hand plot shows the same curves for the analog calorimeter Level 1 algorithm.*

4 Single particle efficiencies.

An important step in understanding the trigger system is the understanding of the response to single particles. For this reason, the simulations used for this study have been extensively tested with single particles (electrons, γ's, μ's) and jets. The results are discussed in this section.

4.1 Electrons and Photons.

Three factors determine the quality of the calorimeter electron/photon trigger algorithm:

1. The trigger efficiency as a function of p_T. In an ideal world, the trigger efficiency should be 0 if p_T is below the trigger threshold and 1 if it is above the threshold.

2. The trigger efficiency as a function of η. This should be constant for the whole detector.

3. The probability that a hadron is misidentified as an electron/photon. This should be small.

The trigger efficiency for single electrons as a function of p_T is plotted in figure 2. This figure shows that the trigger efficiency increases from 0 to > 90% in a range of a few GeV for both calorimeter algorithms. The shape of the threshold curves is (almost) independent of the algorithm and the threshold. The inefficiency at high p_T values is caused by a spurious "hadronic" or "isolation" veto resulting from leakage into the hadronic calorimeter and

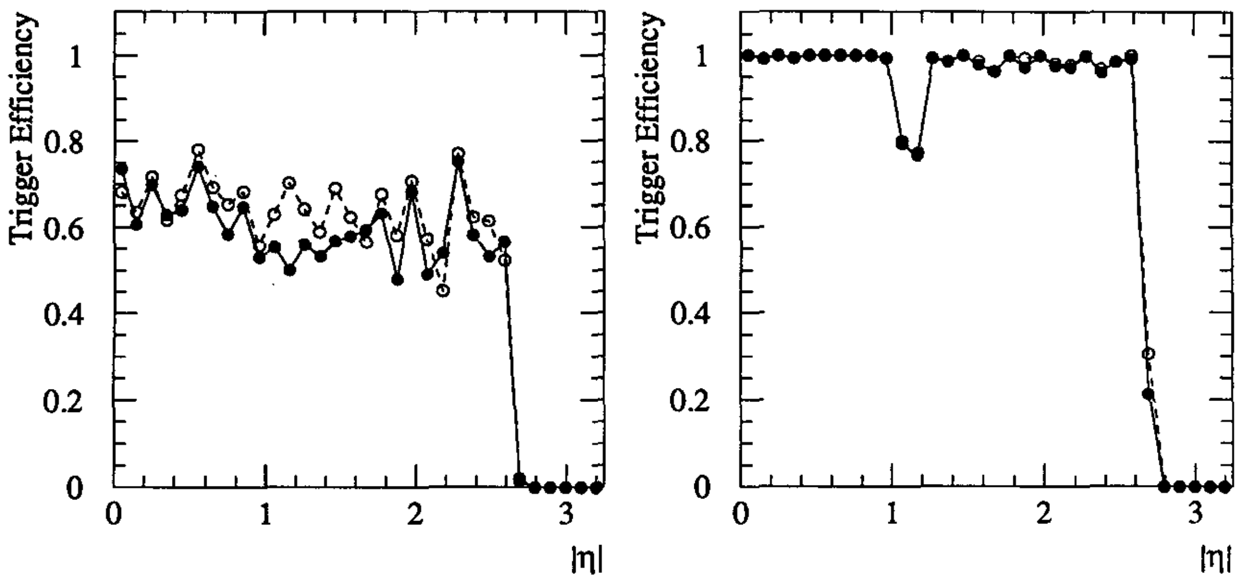

Figure 3: Trigger efficiency for electrons as a function of η. The left hand side plot shows the trigger efficiency of the E_8 e/γ for a p_T of 10 GeV *for the analog (○) and digital (•) calorimeter Level 1 algorithms. The right hand side plot shows the trigger efficiency for a p_T of* 50 GeV.

neighboring electromagnetic cells; it can be improved by changing the constants in the algorithms. It should also be noted that `gemfast` does not precisely model this leakage. The digital algorithm uses more restrictive isolation criteria and will thus be a little more inefficient than the analog algorithm.

Figure 3 shows the trigger efficiency on single electrons as a function of η. For an energy well above the threshold, the efficiency for both algorithms is in general close to 100%. In the transition region between barrel and end-cap calorimeters ($|\eta| \approx 1.1$), the EM resolution is considerably worse than in the rest of the detector. This explains the drop in efficiency at that point. For $|\eta| \gtrsim 2.5$, electromagnetic isolation cannot be tested and no photons or electrons will be found in that region. For an energy just above the threshold, the efficiency drops. This is consistent with the results shown in figure 2.

The probability that a single $\pi^\pm$ is identified as an electron is plotted in figure 4. For $\pi^\pm$'s with a p_T of 50 GeV, there is about a 5 to 10% chance that a particle is misidentified. This probability drops for lower p_T values. This is reasonable number for a Level 1 trigger. The peak in the curve for the analog algorithm at $|\eta| \approx 2.1$ is caused by the transition in cell-size at that point which make the hadronic isolation criteria hard to implement. Presumably most of the misidentified pions can be rejected at Level 2.

The conclusions that can be drawn from these plots are that the performance of both electron/photon trigger algorithms is perfectly acceptable for GEM and the performance of both algorithms is comparable. Fine-tuning of the constants in the algorithms will, presumably, improve the performance even further.

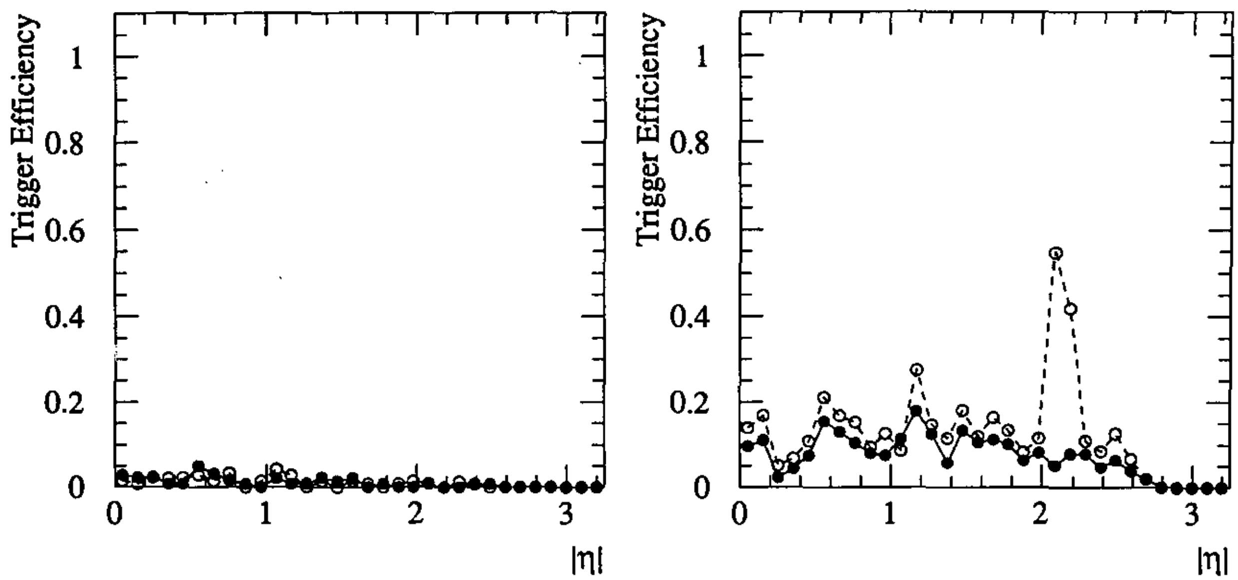

Figure 4: Probability that a $\pi^{\pm}$ is misidentified as an electron by the Level 1 trigger. The left hand side plots shows this probability for $\pi^{\pm}$'s with a p_T of 10 GeV *as a function of η, the right hand side plot shows this probability for a p_T of* 50 GeV. *In both plots,* • *refers to the digital calorimeter Level 1 algorithm and* ○ *to the analog calorimeter Level 1 algorithm.*

4.2 Jets.

The performance of the jet-triggers has also been studied. Figure 5 shows the trigger efficiency for single jets as a function of p_T for both algorithms; the curves are identical. The slower rise of these curves compared with those for electrons is due to the hadronic energy resolution being worse than the electromagnetic energy resolution.

The trigger efficiency as a function of η is shown in figure 6. For jets with a p_T of 100 GeV, the efficiency is about 90%. For lower p_T-values, the efficiency drops. This is consistent with the results presented in figure 5. Except for the region around $|\eta| \approx 2.1$, where the analog algorithm will often misidentify hadrons as electrons, both algorithms produce identical results.

4.3 Muons.

Figure 7 shows the trigger efficiency for the Level 1 muon trigger as a function of η and p_T. The algorithm used to determine the trigger efficiency is described in detail in [13]. The trigger thresholds were chosen such that the trigger is 84% efficient for muons with a p_T equal to the threshold.

The threshold values used in this study are slightly different from the thresholds that have been used in a detailed study of the actual implementation of the muon trigger system [14]. However, the behavior of the muon trigger is determined by the *shape* of the threshold curves and the curves used here are in agreement with the curves calculated in the detailed study. The different threshold values result in small ($\mathcal{O}(10)$%) differences between the trigger

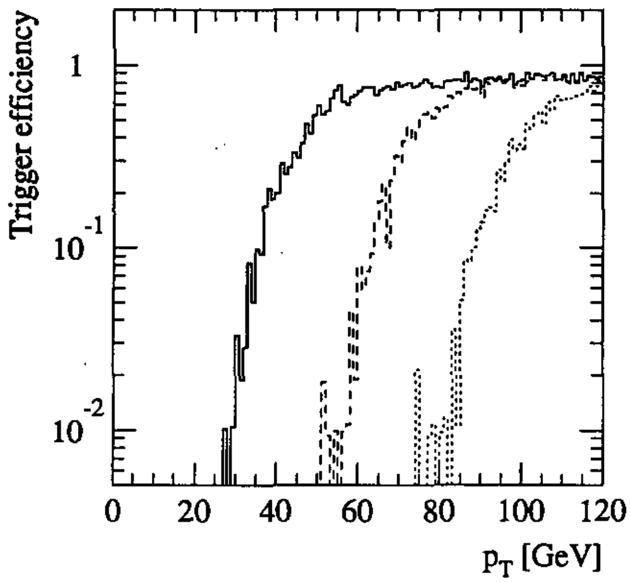

Figure 5: Trigger efficiency for single jets as a function of p_T of the jet trigger, for $0.4 \leq \eta \leq 0.6$. *The left hand plot shows the probability that the digital calorimeter Level 1 algorithm finds at least 1 jet candidate above thresholds of* 25, 50 *and* 75 GeV, *the right hand side plot shows the same curves for the analog calorimeter Level 1 algorithm.*

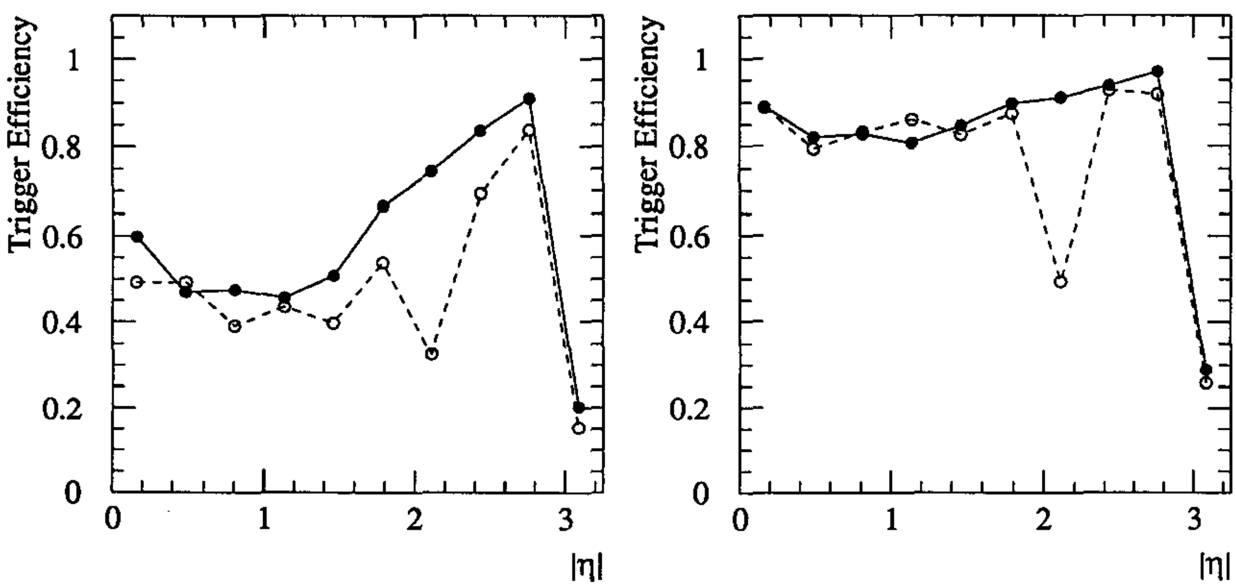

Figure 6: Trigger efficiency for single jets as a function of η. The left hand side plot shows the trigger efficiency of the J_{25} jet trigger for jets with a p_T of 50 GeV *for the analog (○) and digital (●) calorimeter Level 1 algorithms. The right hand side plot shows the efficiency for jets with a p_T of* 100 GeV.

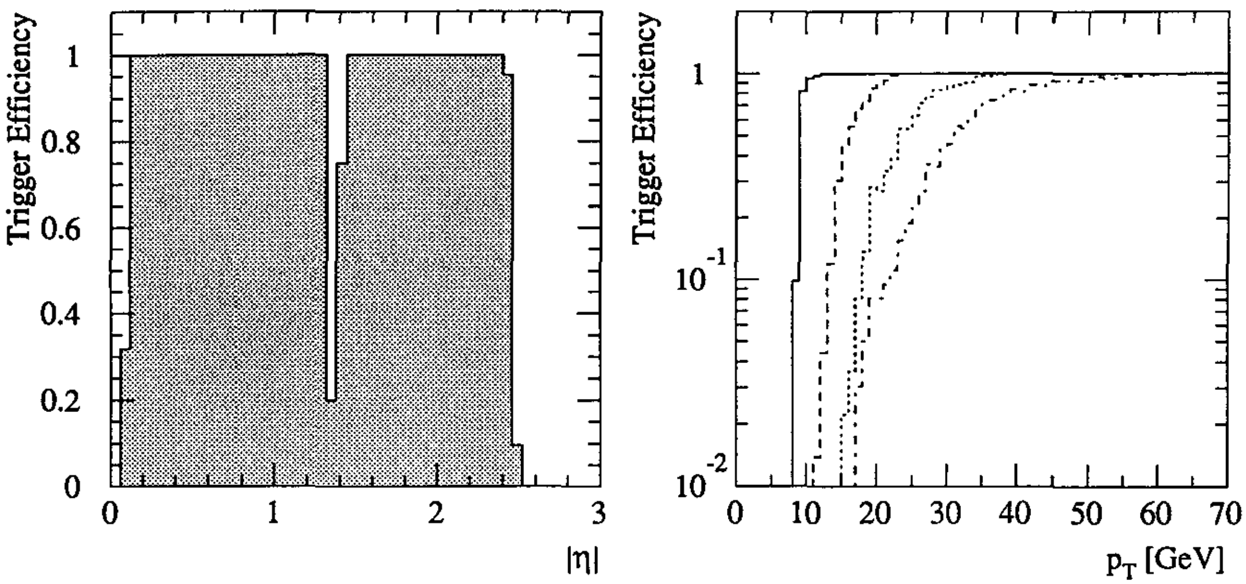

Figure 7: Trigger efficiency of the Level 1 muon trigger. The left hand side plot shows the trigger efficiency as a function of η for μ's with a p_T of 100 GeV *and a threshold of* 10 GeV*. The right hand side plot shows the trigger efficiency as a function of p_T for thresholds of* 10, 20, 30 *and* 40 GeV.

efficiencies for muons of a given p_T. This will not have a significant impact on the final results on physics efficiencies.

The studies presented here do not include false muon triggers. This rate has been calculated independently and is expected to be of the order of 1.1 kHz for a threshold of 20 GeV or 0.3 kHz for a threshold of 30 GeV [14].

5 Physics efficiency and background reduction.

5.1 Physics efficiency.

The trigger efficiency for the processes listed in table 1 was determined using samples of 5000 to 10000 events for every process. The results can be found in table 3.

In general, the trigger efficiency for physics should high, *e.g.* $\gtrsim$ 90%. Table 3 shows that this is the case for most heavy particle production processes. The trigger efficiency is below that level for some of the low-mass H^0-production processes and has to be improved by optimizing the thresholds. This will be discussed in section 6.1.

The numbers for $H^0 \rightarrow \gamma\gamma$ show that trigger efficiency for this process increases by 2.4 to 6.8% when the more restrictive generator level cuts were used (see table 1). This shows that the trigger rejects some fraction of events that cannot be analyzed anyway and that we should not worry about a few percent of inefficiency when tuning the trigger thresholds. The same is true for $t\bar{t}$-production events. The initial trigger efficiency is only 75%. However, if one requires that the event can be analyzed off-line, the trigger efficiency increases to almost

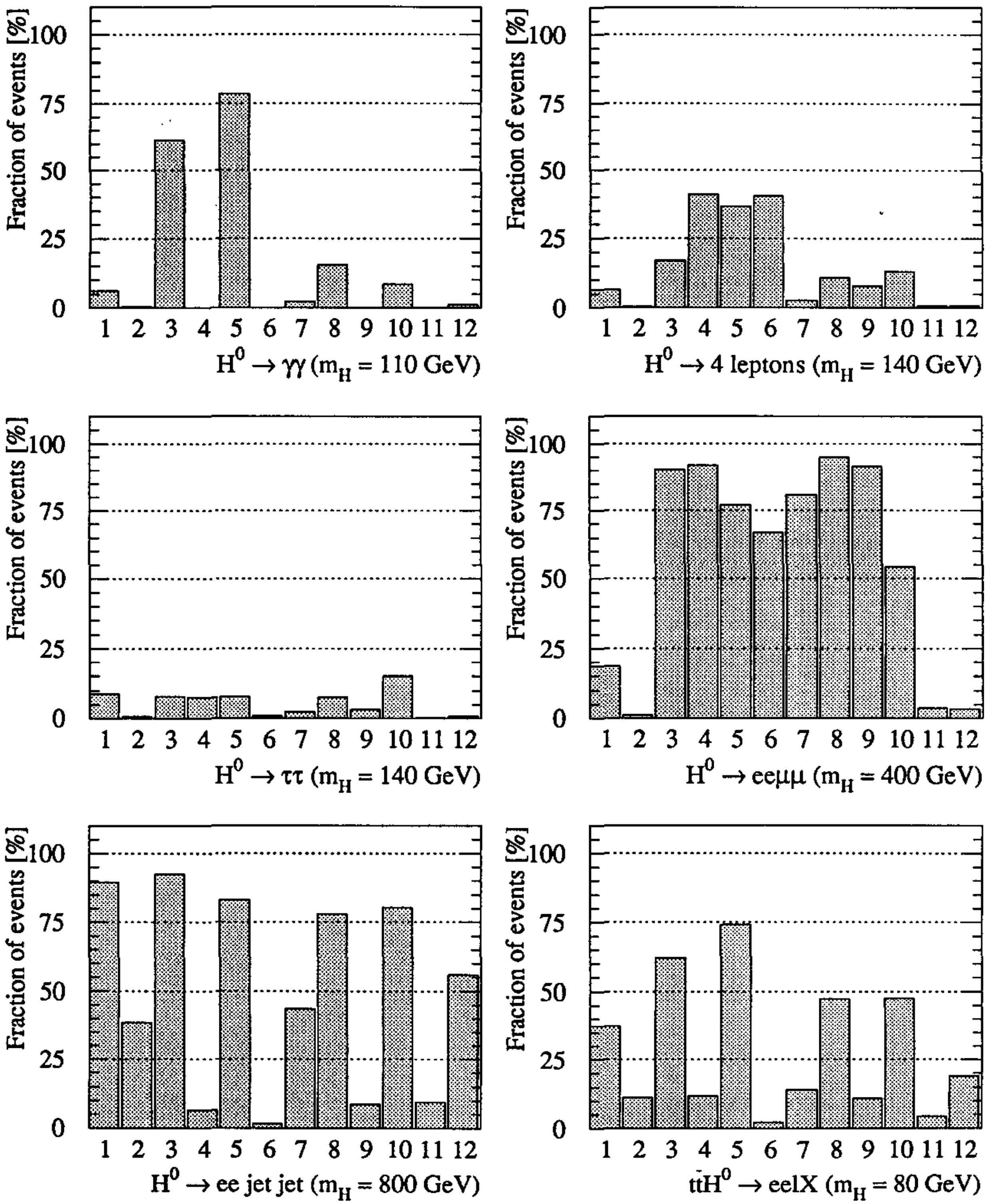

Figure 8: Fraction of accepted events by each of the 12 trigger conditions from table 2 for Higgs events. The global trigger decision is the logical "OR" of the 12 trigger conditions.

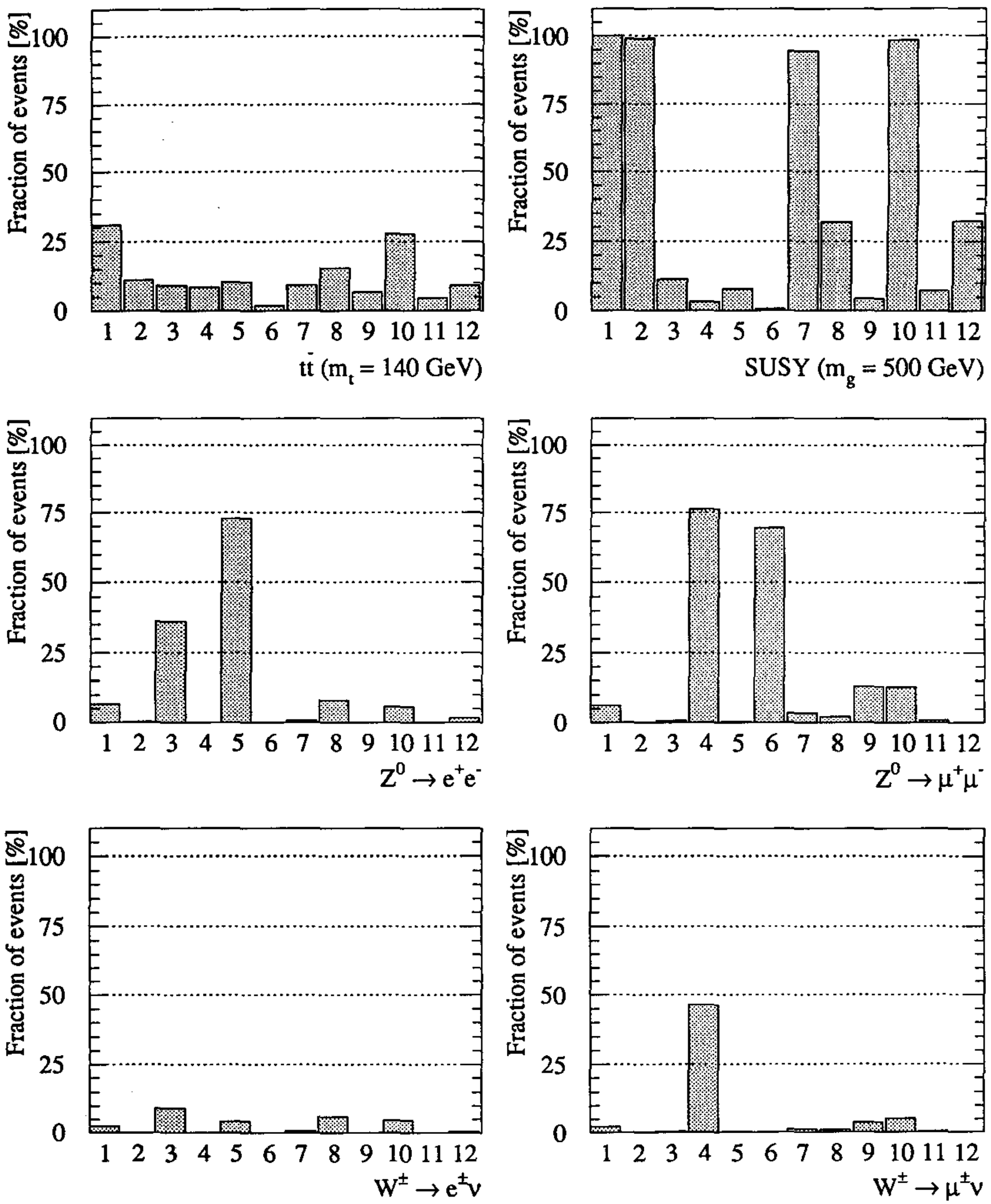

Figure 9: Fraction of accepted events by each of the 12 trigger conditions from table 2 for heavy flavor, SUSY and calibration events. The global trigger decision is the logical "OR" of the 12 trigger conditions.

Process	M_{H^0} [GeV]	# Generated events	Fraction Accepted	Fraction Accepted
$H^0 \to \gamma\gamma$	80	10000	78.82 %	85.61 %
	110	10000	89.31 %	93.24 %
	140	10000	94.66 %	97.08 %
$H^0 \to \tau\tau$	140	10000	34.72 %	
$H^0 \to Z^0Z^* \to \ell^+\ell^-\ell^+\ell^-$	140	10000	81.77 %	
$H^0 \to Z^0Z^* \to e^+e^-e^+e^-$	140	10000	83.34 %	
$H^0 \to Z^0Z^* \to \mu^+\mu^-\mu^+\mu^-$	140	10000	86.38 %	
$H^0 \to Z^0Z^* \to e^+e^-\mu^+\mu^-$	140	10000	78.68 %	
$H^0 \to Z^0Z^0 \to e^+e^-\mu^+\mu^-$	400	10000	99.80 %	
$H^0 \to Z^0Z^0 \to e^+e^-$jet jet	800	10000	99.85 %	
$H^0 \to Z^0Z^0 \to e^+e^-\nu\overline{\nu}$	800	5000	98.88 %	
$H^0 \to Z^0Z^0 \to \mu^+\mu^-\nu\overline{\nu}$	800	5000	94.18 %	
$t\bar{t} + H^0 \to \ell\gamma\gamma + X$	80	9981	94.38 %	
$t\bar{t}$-production.		10000	75.23 %	
SUSY, $\tilde{g}\tilde{g}$-production.		10000	99.99 %	
$W^\pm \to e\nu$		10000	15.92 %	
$W^\pm \to \mu\nu$		10000	48.73 %	
$Z^0 \to e^+e^-$		10000	80.35 %	
$Z^0 \to \mu^+\mu^-$		10000	86.88 %	

Table 3: Physics efficiency for the Level 1 trigger criteria suggested in table 2. The fourth column lists the trigger efficiency when the standard generator cuts were used, the fifth column the efficiency when more restrictive generator cuts were used. (See table 1).

100% [15].

The trigger efficiency for Z^0- and $W^\pm$-production also seems low. But this is not a problem as these events are mainly used for calibration purposes and the production rate is high.

Figures 8 and 9 show the fraction of events accepted by each trigger condition. These figures show that events for a specific process are indeed accepted with good efficiencies by the triggers that were intended for that process. This implies that reasonable assumptions were made in [1].

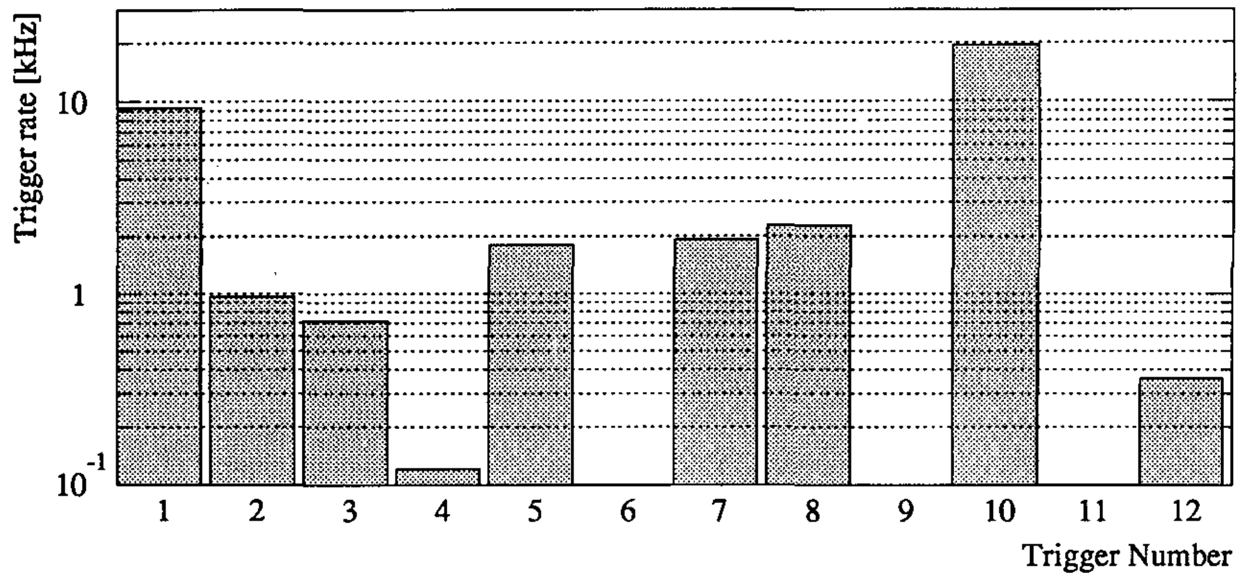

Figure 10: Trigger rate for the 12 trigger conditions from table 2 for minimum bias background events.

5.2 Background reduction.

A total of 5×10^5 minimum bias events were generated. Only 207 of them satisfied at least one of the trigger conditions and were accepted by the trigger. This corresponds in a background reduction from 60 MHz to 24.8 kHz. Even for our pessimistic estimate of the background rate, this is already close to the design goal for the Level 1 trigger of $\mathcal{O}(10)$ kHz.

The trigger rate of the individual trigger modes is shown in figure 10. This figure shows that most of the events are accepted by the single jet trigger and the jet and $\not{E}_T$ trigger. Increasing the thresholds of these triggers will have the biggest impact on the background rate. This is discussed in section 6.1.

6 Optimization of the trigger.

In general, there are two methods to increase the physics efficiency of a trigger:

1. Lowering the thresholds of specific trigger conditions.

2. Adding more trigger conditions, to cover other final states.

Unfortunately, reducing the background rate involves exactly the opposite:

1. Increasing the thresholds of specific trigger conditions.

2. Decreasing the number of trigger conditions and/or pre-scaling them. Pre-scaling means that only a fraction of the events satisfying a trigger condition is actually accepted.

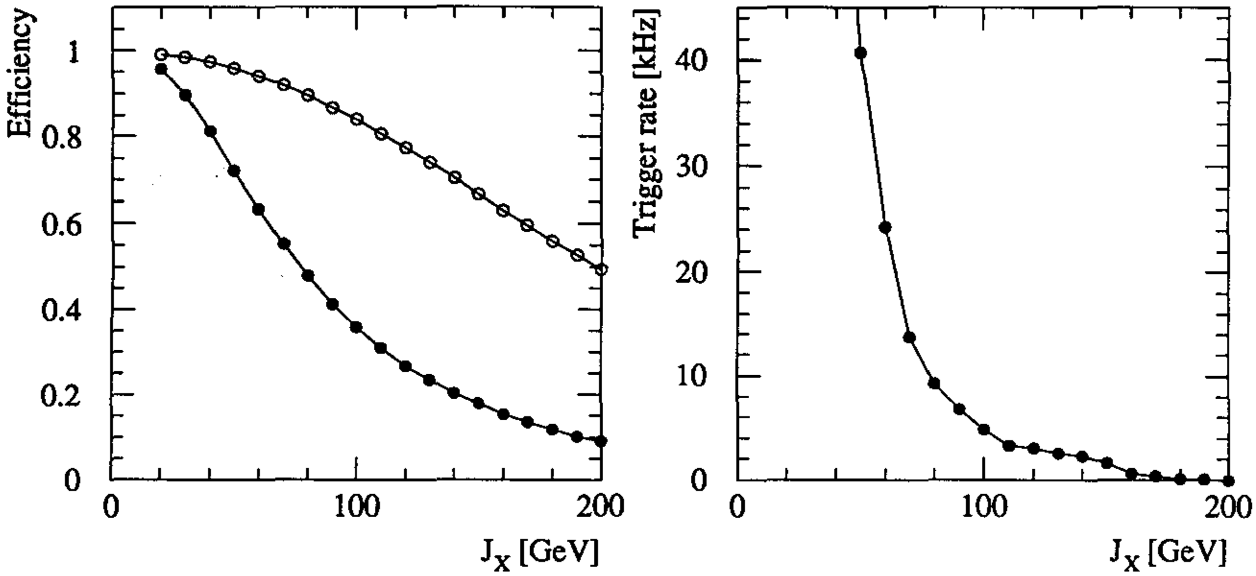

Figure 11: The left hand side plot shows the trigger efficiency as a function of the threshold for a single jet trigger (J_x) for $t\bar{t}$-production (•) and $H^0 \rightarrow ee$ jet jet (∘) events. The right hand side plot shows the corresponding minimum bias background rate.

Changing the thresholds will be discussed in section 6.1. Sections 6.2 and 6.3 will discuss two new trigger conditions for final states not considered in [1].

6.1 Changing the thresholds.

Figures 11 through 18 show the background rates as a function of the thresholds for all trigger conditions except the muon triggers #4 and #6 (see table 2). These figures also show the trigger efficiency for one or two processes for which this specific trigger was designed. The muon trigger rates are not plotted here because their trigger rate mainly depends on effects not simulated in `gemfast`.

The trigger rates plotted in figures 11 through 18 do not include events that are already accepted by other trigger conditions. Although this makes the plots perfectly suitable for understanding the behavior of a single trigger, the disadvantage of this method is that the plots do not show what happens to the *overall* trigger rate as a function of the threshold. The rate has to be calculated separately after each change in the thresholds.

We now try to optimize the thresholds. As a first step, we adjust the threshold so that the rate of every trigger condition is about 1 kHz. This requires the following changes:

- Increase the single jet trigger threshold to 150 GeV.
- Increase the $\not{E}_T$ trigger threshold to 125 GeV.
- Lower the muon and $\not{E}_T$ trigger threshold to 25 GeV.
- Lower the single muon threshold to 20 GeV.

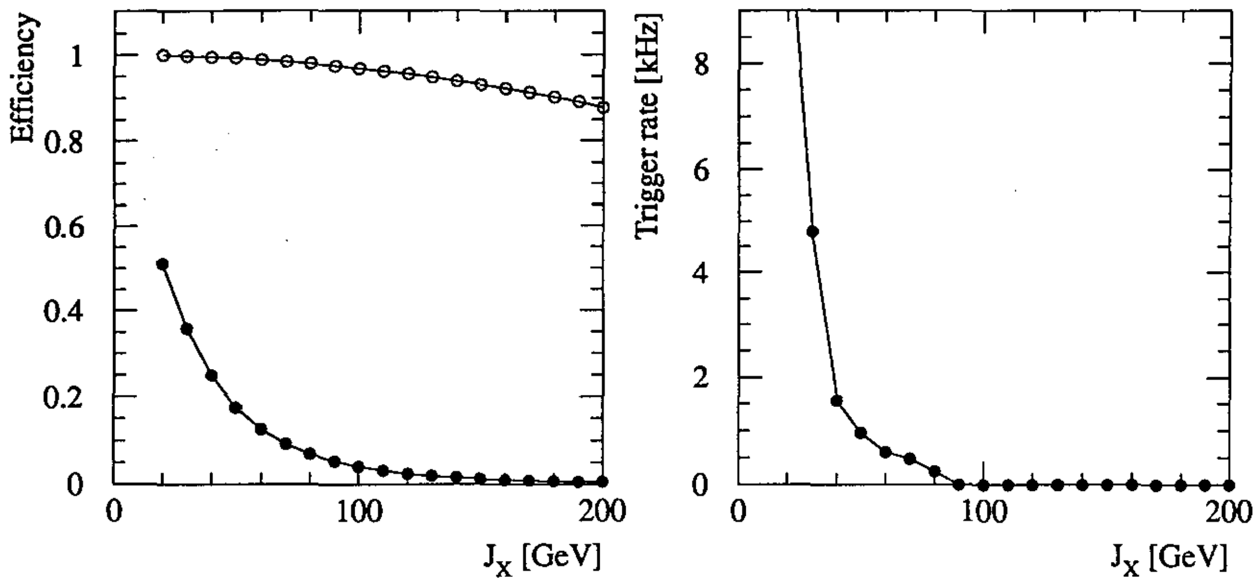

Figure 12: The left hand side plot shows the trigger efficiency as a function of the threshold for a four jet trigger (4 of J_x) for $t\bar{t}$-production (•) and SUSY events (○). The right hand side plot shows the corresponding minimum bias background rate.

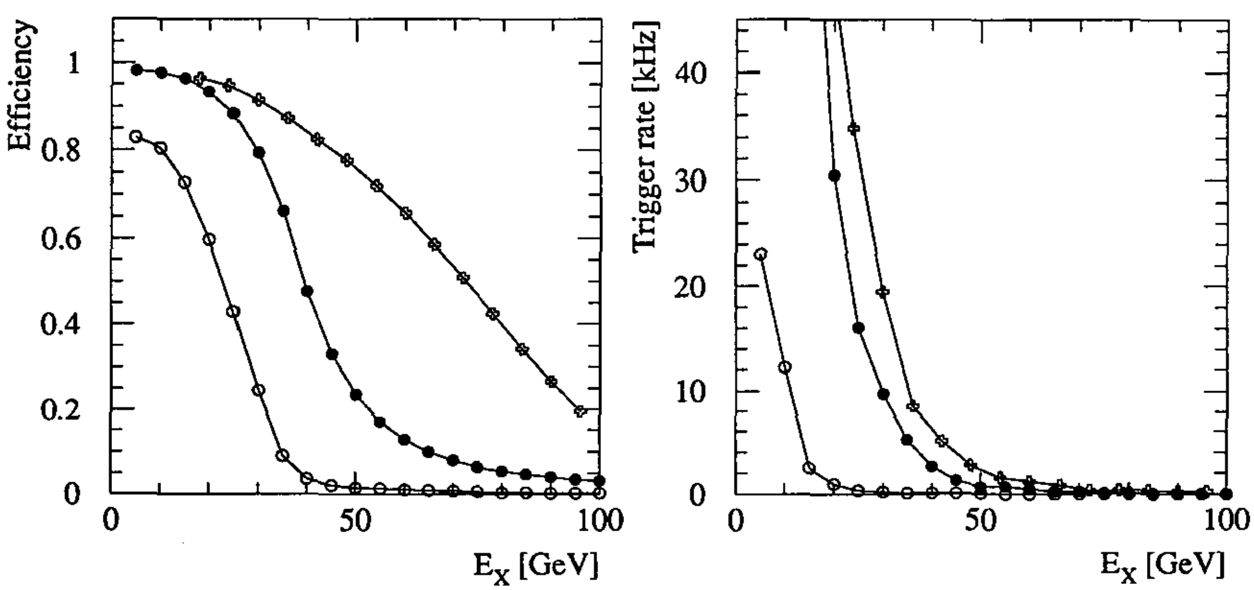

Figure 13: The left hand plot shows the trigger efficiency as a function of the threshold for $H^0 \rightarrow \gamma\gamma$ ($M_{H^0} = 80$ GeV) events. Three cases have been plotted: a single electron/photon trigger (E_x) (•), a two electron/photon trigger (2 of E_x) (○) and a combined one and two photon trigger (E_x OR (2 of $E_{\frac{x}{3}}$)) (+). The right hand side plot shows the corresponding minimum bias background rates.

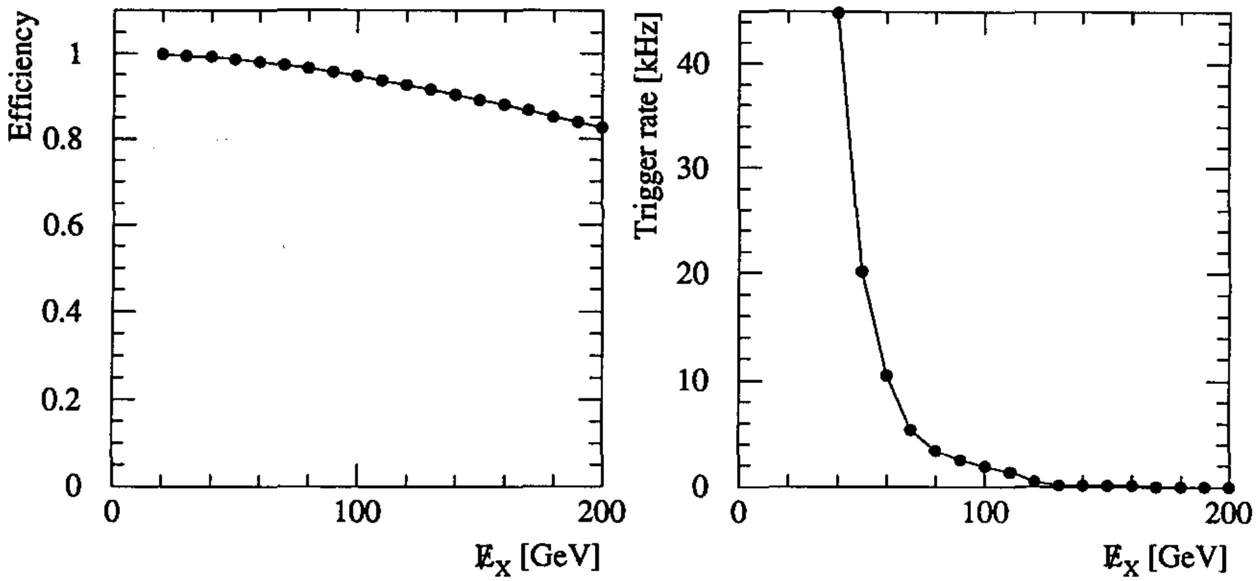

Figure 14: The left hand side plot shows the trigger efficiency as a function of the threshold for an $\not{E}_x$ trigger for SUSY events. The right hand side plot shows the corresponding minimum bias background rate.

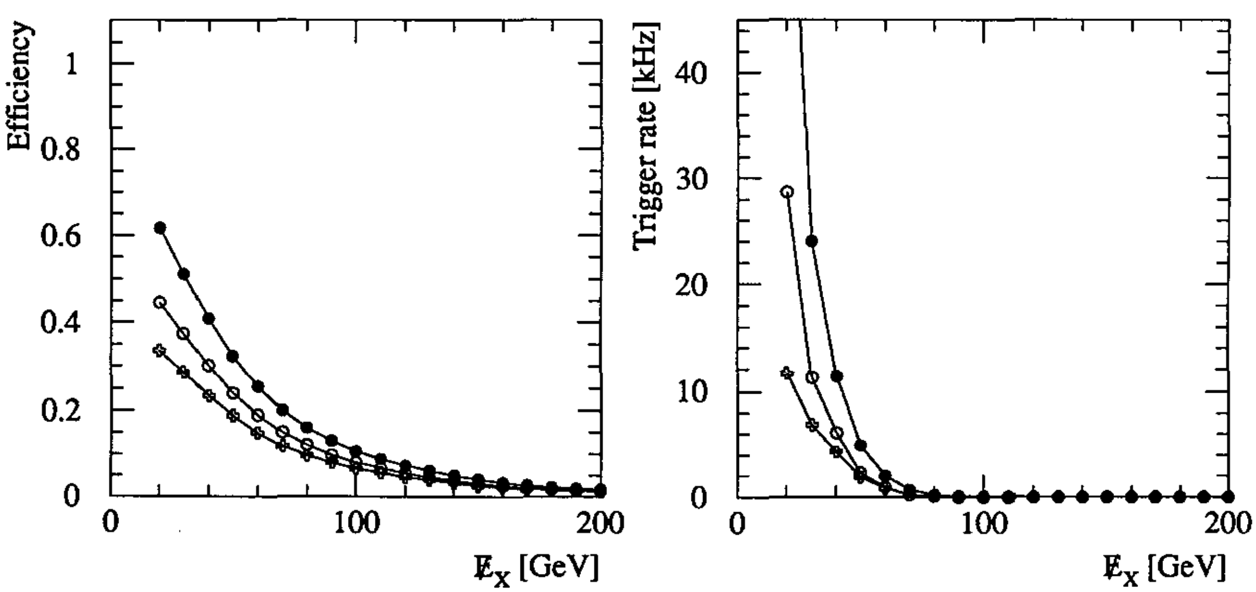

Figure 15: The left hand side plot shows the trigger efficiency for an electron and $\not{E}_T$ trigger (E_y AND $\not{E}_x$) for y = 8 GeV (•), 16 GeV (∘) and 24 GeV (+) as a function of the $\not{E}_T$-threshold for $t\bar{t}$-production events. The right hand side plot shows the corresponding minimum bias background rates.

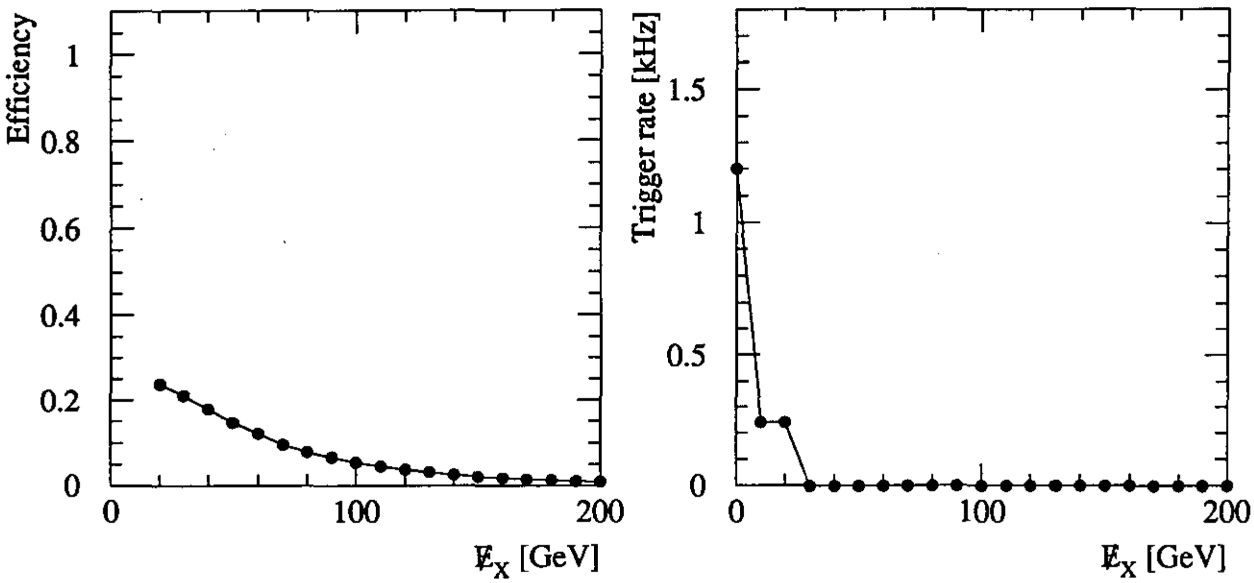

Figure 16: The left hand side plot shows the trigger efficiency for a muon and $\not{E}_T$ trigger (M_{10} AND $\not{E}_x$) as a function of the $\not{E}_T$-threshold for $t\bar{t}$-production events. The right hand side plot shows the corresponding minimum bias background rate.

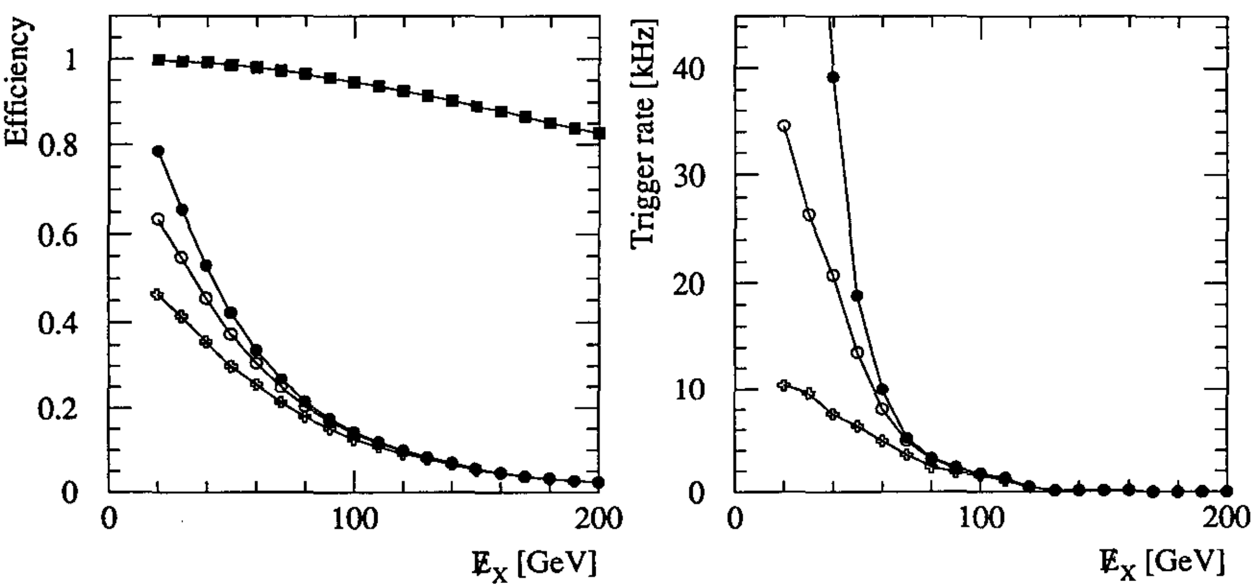

Figure 17: The left hand side plot shows the trigger efficiency for a jet and $\not{E}_T$ trigger (J_y AND $\not{E}_x$) as a function of the $\not{E}_T$-threshold. The curves refer to SUSY events with $y = 25$ GeV (■) and to $t\bar{t}$-events with $y = 25$ GeV (•), 50 GeV (○) and 75 GeV (+). The right hand side plot shows the corresponding minimum bias background rates.

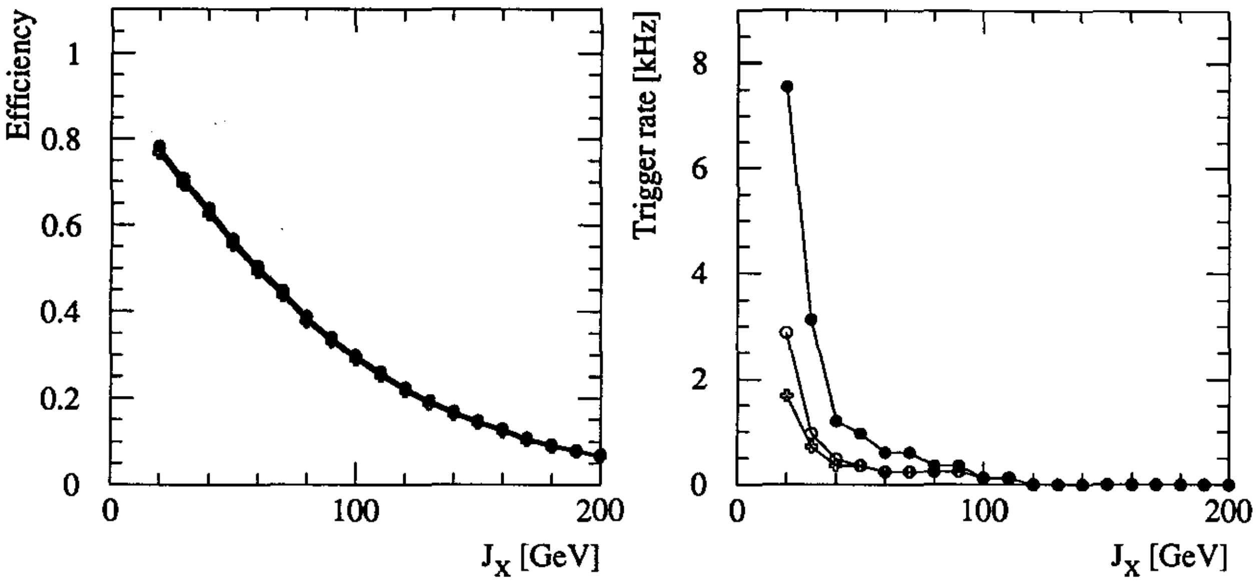

Figure 18: The left hand side plot shows the trigger efficiency for an electron and 3 jet trigger (E_y AND (3 of J_x)) for $y = 8$ GeV (•), 16 GeV (∘) and 24 GeV (+) for $H^0 \rightarrow ee$ jet jet events as a function of the jet-threshold. The right hand side plot shows the corresponding minimum bias background rates.

No.	Trigger	Comment
1	J_{150}	High P_T-jet.
2	(4 of J_{50})	Multi jet event.
3	E_{36}	High P_T electron or γ.
4	M_{20}	High P_T μ.
5	(2 of E_{12})	Two electrons or γ's.
6	(2 of M_{10})	Two μ's.
7	$\not{E}_{125}$	$\not{E}_T$.
8	E_{12} and $\not{E}_{50}$	Electron and $\not{E}_T$ ($W^\pm$, τ)
9	M_{10} and $\not{E}_{25}$	Muon and $\not{E}_T$ ($W^\pm$, τ)
10	-	-
11	M_{10} and (3 of J_{25})	Muon and 3 jets.
12	E_{12} and (3 of J_{25})	Electron and 3 jets.

Table 4: Modified Level 1 trigger criteria. Refer to table 2 for the notation.

Process	*Fraction Accepted*		
	Original	*Step 1*	*Step 2*
$H^0 \to \gamma\gamma$ ($m_{H^0} = 80$ GeV)	78.82 %	78.57 %	88.02 %
$H^0 \to e^+e^-$jet jet	99.85 %	99.66 %	99.73 %
$t\bar{t}$-production.	75.23 %	70.05 %	76.33 %
SUSY, $\tilde{g}\tilde{g}$-production.	99.99 %	99.99 %	99.99 %
Background rate.	24.8 kHz	7.4 kHz	15.0 kHz

Table 5: Trigger rates for the modified set of trigger conditions. The column labeled "original" shows the rates for the conditions listed in table 2, the column labeled "step 1" the rates using the conditions from table 4 before the photon trigger thresholds are lowered and the column labeled "step 2" the rates using these conditions after the photon trigger thresholds are lowered.

- Remove the jet and $\not{E}_T$ trigger.
- Lower the lepton and 3 jet trigger thresholds to 25 GeV. The value of 25 GeV is equal to the lowest jet energy that can be reliably measured by the calorimeter Level 1 trigger. Currently, this value is of the order of 25 GeV [16].

Table 4 shows the modified set of trigger conditions. These modifications reduces the minimum bias background rate by a factor of 3 to 7.4 kHz with, see table 5, only small changes in the physics efficiency. The rate of 7.4 kHz is below the Level 1 design value. This suggests that we can lower some of the thresholds again. The next modifications therefore are:

- Lower the single photon trigger threshold to 36 GeV.
- Lower the two photon trigger threshold to 12 GeV.

This will improve the efficiency for low-mass H^0-events. These changes increase the $H^0 \to \gamma\gamma$ ($m_{H^0} = 80$ GeV) efficiency for by about 10% but also increase the background rate to 15.0 kHz, see table 5 for details.

Tuning the trigger thresholds is an iterative process. The next step therefore is to plot the trigger rates for every trigger mode and process again and tune the thresholds even further. This optimization process has to be repeated until the optimal combination of thresholds has been found. But, at this stage of the experiment, this exercise is not particularly useful.

The important conclusion that can be drawn from this section is that with some tuning of the thresholds the background rate *even for a pessimistic estimate of the rate* can be reduced to a level acceptable for the Level 1 trigger while at the same time providing enough efficiency for physics.

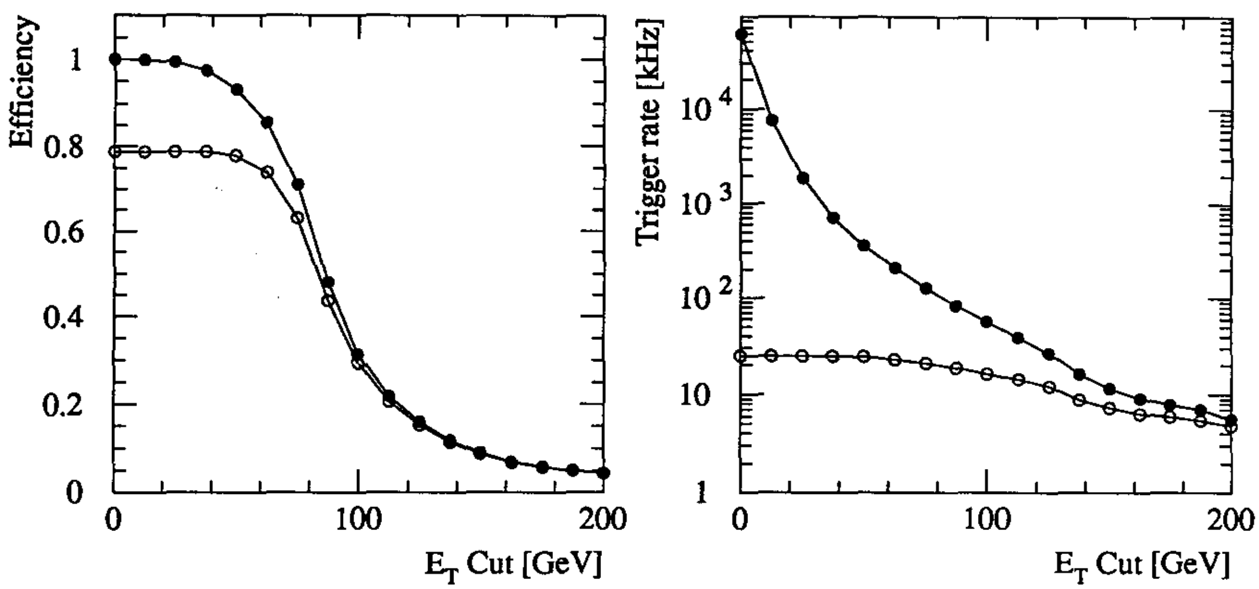

Figure 19: The left hand side plot shows the trigger efficiency as a function of an E_T-cut for $H^0 \rightarrow \gamma\gamma(m_{H^0} = 80$ GeV) before (•) and after (○) the cuts of table 2 have been applied. The right hand side plot shows the corresponding minimum bias background rates.

6.2 Scalar E_T-triggers.

The only trigger primitive that is not used in our list of trigger conditions is E_T. An E_T trigger can be used as a global trigger on the activity in the detector.

Figure 19 shows the efficiency for a typical physics process ($H^0 \rightarrow \gamma\gamma$) and the corresponding minimum bias background rate as a function of an E_T cut. From this figure it can be seen that an E_T cut *alone* cannot reduce the background by 4 orders of magnitude without seriously affecting the physics performance of the detector.

However, a modest E_T-cut of about 40 GeV gives two orders of magnitude in background reduction without any loss in physics acceptance. This suggests that a trigger where an E_T-cut is logically "AND"-ed with other trigger conditions might be of interest, *e.g.* one triggers on detector activity *and* a specific event signature.

The performance of such a trigger is also plotted in figure 19. The figure shows that the background rate after the other trigger criteria have been applied is almost independent of E_T and it is therefore not possible to reduce the rate without affecting the physics acceptance.

The conclusions that can be drawn from this study are that our trigger conditions have implicit E_T-requirements and that scalar E_T-triggers are of very limited use for GEM.

6.3 Electron/muon triggers.

The triggers for the processes $H^0 \rightarrow e^+e^-e^+e^-$ and $H^0 \rightarrow \mu^+\mu^-\mu^+\mu^-$ require that two of the four electrons or muons are found. These conditions allow for some trigger inefficiency without affecting the performance for this processes. But any trigger inefficiency will affect

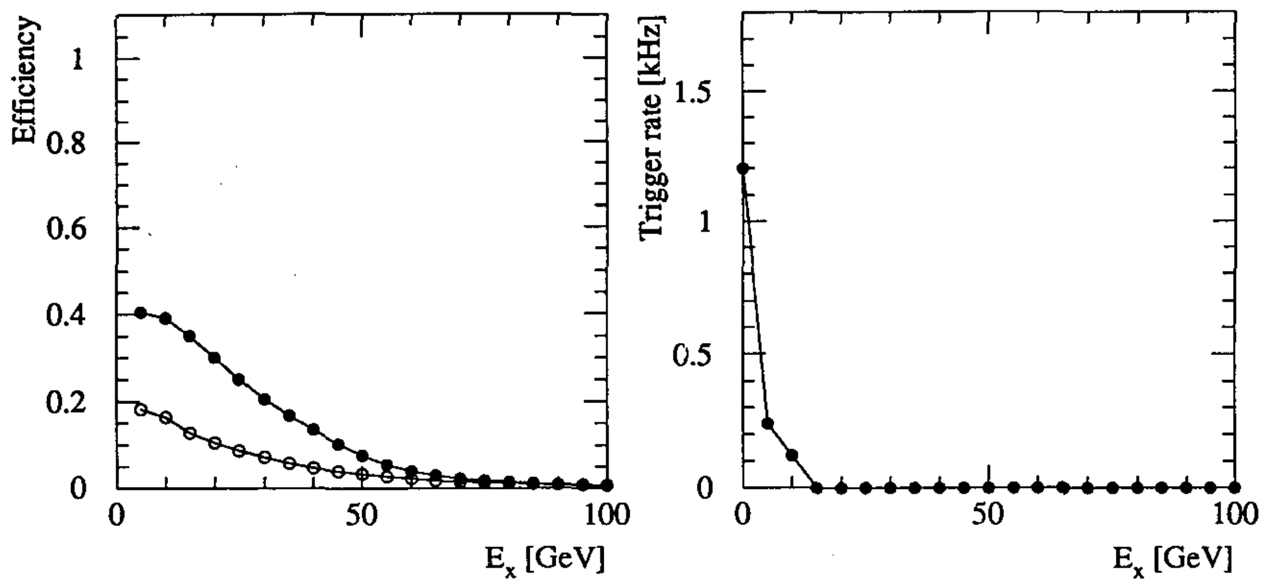

Figure 20: The left hand side plots shows the trigger efficiency for an electron-muon-trigger (E_x AND M_{10}) as a function of the electron threshold for $H^0 \rightarrow \ell\ell\ell\ell$ (•) and $t\bar{t}$-production events (∘). The right hand side plot shows the corresponding minimum bias background rates.

the process $H^0 \rightarrow e^+e^-\mu^+\mu^-$ since the trigger cannot recover from a situation where it misses one of the electrons or muons.

An electron-muon trigger (E_x *AND* M_{10}) might be able to recover those events. Figure 20 shows the efficiency for this trigger condition and the corresponding minimum bias background rate. The figure shows that, for a threshold of $x = 16$ GeV, about 35% out of a possible 50% of the $H^0 \rightarrow \ell\ell\ell\ell$ events will be accepted by this trigger without any increase in the background rate.

Some of the events accepted by this new trigger will, of course, also be accepted by the muon- and electron-pair triggers. Adding this trigger to the list of 12 trigger increases the overall efficiency by 6.5%.

This trigger will also accept events like

$$t\bar{t} \rightarrow W^+b\, W^-\bar{b} \rightarrow e^+\text{jet}\ \mu^-\text{jet}$$

and increase the efficiency for these kinds of events.

The conclusion that can be drawn is that the trigger (E_x *AND* M_{10}) is a background-free trigger that gives some improvement in the performance for multi-lepton final states.

6.4 The modified set of triggers.

Combining the results from section 6.1 and 6.3 leads to an optimized set of trigger criteria, see table 6.

The physics efficiencies for this set of trigger criteria has been determined and is listed in table 7. Comparing these results with the result using the original set of thresholds (table 3)

No.	Trigger	Comment
1	J_{150}	High P_T-jet.
2	(4 ofJ_{50})	Multi jet event.
3	E_{36}	High P_T electron or γ.
4	M_{20}	High P_T μ.
5	(2 ofE_{12})	Two electrons or γ's.
6	(2 ofM_{10})	Two μ's.
7	$\not{E}_{125}$	$\not{E}_T$.
8	E_{12} and $\not{E}_{50}$	Electron and $\not{E}_T$ ($W^{\pm}$, τ)
9	M_{10} and $\not{E}_{25}$	Muon and $\not{E}_T$ ($W^{\pm}$, τ)
10	-	-
11	M_{10} and (3 ofJ_{25})	Muon and 3 jets.
12	E_{12} and (3 ofJ_{25})	Electron and 3 jets.
13	M_{10} and E_{12}	Electron and muon trigger.

Table 6: Optimized Level 1 trigger criteria. Refer to table 2 for the notation.

shows a clear improvement, in particular for low-mass H^0-events.

The trigger efficiency is, in general, close to or above the 90% level. The only exception is the efficiency for $H^0 \rightarrow \tau\tau$-events. This can be explained from the fact that the trigger intended for hadronic τ-decays (J_{12} *AND* $\not{E}_{50}$) does not work as planned: it only accepts a few τ's and it is the dominating source of accepted background events. This problem can probably be solved by introducing special τ-triggers. This will be discussed in a future note.

The minimum bias background rate for the optimized set of trigger criteria is 15.0 kHz. As has been mentioned before, our estimate of this rate can be up to a factor of 2 too high. The false muon trigger rate, see section 4.3, for these thresholds is about 1.1 kHz. This is not included in this number.

7 Conclusions and outlook.

The optimized set of trigger criteria presented in table 6 has a high physics acceptance and at the same time reduces the backgrounds to an acceptable level. Fine-tuning of the thresholds, as well as the constants used in algorithms, will further increase the performance.

The only process for which the acceptance is not acceptable is $H^0 \rightarrow \tau\tau$. This probably can be solved by adding dedicated τ-triggers to the list of triggers and has to be studied.

The events sample used here covers most of the physics program for GEM at $\mathcal{L} = 10^{33}\text{cm}^{-2}\text{s}^{-1}$. Triggering at $\mathcal{L} = 10^{34}\text{cm}^{-2}\text{s}^{-1}$ should also be studied. Also more trigger hardware details, which will become available as the design of the systems evolves, will be added to the simulation and the effect on the trigger performance studied.

In parallel with the Level 1 studies, work will be done on Level 2 and Level 3 trigger algorithms. Figure 4, for example, suggests that the Level 2 trigger should repeat the

Process	M_{H^0} [GeV]	*# Generated events*	*Fraction Accepted*	*Fraction Accepted*
$H^0 \to \gamma\gamma$	80	10000	88.02 %	92.88 %
	110	10000	94.36 %	97.12 %
	140	10000	96.54 %	98.09 %
$H^0 \to \tau\tau$	140	10000	42.57 %	
$H^0 \to Z^0 Z^* \to \ell^+\ell^-\ell^+\ell^-$	140	10000	87.72 %	
$H^0 \to Z^0 Z^* \to e^+e^-e^+e^-$	140	10000	86.86 %	
$H^0 \to Z^0 Z^* \to \mu^+\mu^-\mu^+\mu^-$	140	10000	88.82 %	
$H^0 \to Z^0 Z^* \to e^+e^-\mu^+\mu^-$	140	10000	87.60 %	
$H^0 \to Z^0 Z^0 \to e^+e^-\mu^+\mu^-$	400	10000	99.83 %	
$H^0 \to Z^0 Z^0 \to e^+e^-$jet jet	800	10000	99.73 %	
$H^0 \to Z^0 Z^0 \to e^+e^-\nu\bar{\nu}$	800	5000	98.30 %	
$H^0 \to Z^0 Z^0 \to \mu^+\mu^-\nu\bar{\nu}$	800	5000	94.00 %	
$t\bar{t} + H^0 \to \ell\gamma\gamma + X$	80	9981	96.94 %	
$t\bar{t}$-production.		10000	76.39 %	
SUSY, $\tilde{g}\tilde{g}$-production.		10000	99.99 %	
$W^\pm \to e\nu$		10000	35.32 %	
$W^\pm \to \mu\nu$		10000	74.80 %	
$Z^0 \to e^+e^-$		10000	88.16 %	
$Z^0 \to \mu^+\mu^-$		10000	92.18 %	

Table 7: Physics efficiency for the Level 1 trigger criteria suggested in table 6. The fourth column lists the trigger efficiency when the standard generator cuts were used, the fifth column the efficiency when more restrictive generator cuts were used. (See table 1).

electron/photon finding with more restrictive cuts to get rid of $\pi^\pm$'s misidentified as electrons. Several other suggestions for Level 2 algorithms have been made, see [17]. All ideas still have to be simulated and tested; some studies may require full GEANT (*e.g.* non-parameterized) simulations. Work in this area is in progress and will be described in a future note.

List of Figures

List of Tables

References

[1] K. McFarlane, H. Uijterwaal; GEM TN 93-294.

[2] GEM collaboration; Technical Design Report, 1993.

[3] H. Uijterwaal; in section 7.2.4. of reference [2].

[4] T. Sjöstrand; PYTHIA, CERN–TH 6488/92.

[5] F. E. Paige, S. D. Protopopescu; ISAJET, BNL–38774 (1986).

[6] I. Sheer; GEM TN 93-379.

[7] T. Skwarnicki; `gemfast`, fast simulation of the GEM detector, version II 2.03.

[8] D. Groom; SSC–N–154.

[9] S. Mrenna; in section 2.3.4. of reference [2].

[10] H. Yamamoto; in section 2.3.3. of reference [2].

[11] H. Uijterwaal; `libtrf`, trigger simulation for `gemfast`, version 1.03.

[12] Bill Cleland; Results presented at the February 1993 trigger and DAQ meeting at the SSCL.

[13] P. Dingus, Y. N. Guo, H. Uijterwaal; GEM TN 93-394.

[14] M. Atiya; in section 4.2.1 of reference [2].

[15] C. Yanigasawa; in section 2.4. of reference [2].

[16] M. Clemen, B. Cleland; private communication.

[17] H. Uijterwaal; in section 7.2.5. of reference [2].

A PYTHIA generator parameters.

This appendix gives an overview of the parameters used to generate events with PYTHIA (see table 1). A detailed description of the parameters can be found in reference [4].

A.1 Processes and subprocesses.

The following table lists the selected processes (MSEL) and subprocesses (MSUB).

Event type	MSEL	MSUB
$H^0 \to \gamma\gamma$.	16	–
$H^0 \to \tau\tau$.	16	–
$H^0 \to Z^0 Z^* \to \ell^+\ell^-\ell^+\ell^-$.	0	102, 123, 124.
$t\bar{t} + H^0 \to \ell\gamma\gamma + X$.	0	121, 122
$t\bar{t}$-production.	6	82
$W^\pm \to \ell^\pm\nu$.	0	2, 16, 20, 31, 36
$Z^0 \to \ell^+\ell^-$.	0	15, 19, 30
Minimum Bias.	0	92, 93, 95

A.2 Kinematic cuts.

The following table lists the kinematic cuts (CKIN) used to generate the events for each process. If no value is specified, the default setting has been used. Lower limits are indicated with a $-$-sign in the parameter name, upper limits are indicated with a $+$-sign in the parameter name.

	CKIN-index.								
	1	2	5	13	14	17	18	45	46
Event type			6	15	16	19	20	47	48
	$\sqrt{S^-}$	$\sqrt{S^+}$	p_T^-	η^-	η^+	$\cos\theta^-$	$\cos\theta^+$	$m_{Z^0}^-$	$m_{Z^0}^+$
$H^0 \to \gamma\gamma$ (Sample 1).				-3	3				
(Sample 2).			20	-2.5	2.5	-0.7	0.7		
$H^0 \to \tau\tau$.				-3	3				
$H^0 \to Z^0 Z^* \to \ell^+\ell^-\ell^+\ell^-$.	130	150						10	120
$t\bar{t}$-production.				-3	3				
$W^\pm \to \ell^\pm\nu$.				-2.5	2.5				
$Z^0 \to \ell^+\ell^-$.				-2.5	2.5				

A.3 Particle decay modes.

The following tables shows the allowed decay modes (MDME) for the produced particles. If no decay modes are specified, the default settings were used for that type of events.

Event type	MDME H^0	MDME Z^0	MDME $W^\pm$	MDME $t,\bar{t}$
$H^0 \to \gamma\gamma$.	197			
$H^0 \to \tau\tau$.	194			
$H^0 \to Z^0 Z^* \to \ell^+\ell^-\ell^+\ell^-$.	199	156 and/or 158		
$t\bar{t} + H^0 \to \ell\gamma\gamma + X$.	197			
$t\bar{t}$-production.				44, 45 and 46
$W^\pm \to \ell^\pm \nu$.			180 or 181	
$Z^0 \to \ell^+\ell^-$.		156 or 158		

A.4 Miscellaneous

The following table shows all other parameters that were set to non-default values.

Parameter name	MDCY	MSTJ		PARJ			
Parameter index	C111	11	22	54	55, 56	73	74
Event type.							
$t\bar{t} + H^0 \to \ell\gamma\gamma + X$.	0	3	4	-0.07	-0.008	20.	10000.
All others.	0		4			20.	10000.

B ISAJET generator parameters.

This appendix gives an overview of the data-cards used to generate events with ISAJET (see table 1). A detailed description of the parameters can be found in reference [5].

B.1 $H^0 \to ee\mu\mu$.

```
SAMPLE HIGGS JOB FOR SSC
40000, 10000, 0, 0/
HIGGS
QMH       200,600/
HMASS     400/
JETTYPE1 'ZO'/
JETTYPE2 'ZO'/
WMODE1    'MU+', 'MU-'/
WMODE2    'E+', 'E-'/
PT        50,   20000,   50,   20000/
Y         -3.0,      3.0, -3.0,      3.0/
```

B.2 $H^0 \to ee\, jet\, jet$.

```
SAMPLE HIGGS JOB FOR SSC
40000, 10000, 0, 0/
HIGGS
QMH       400, 1200/
HMASS     800/
```

```
JETTYPE1 'Z0'/
JETTYPE2 'Z0'/
WMODE1   'QUARKS','QUARKS'/
WMODE2   'E+','E-'/
PT        50,   20000,   50,   20000/
Y        -3.0,     3.0, -3.0,     3.0/
```

The datacard "WMODE1" was replaced with "WMODE1 'NUS', 'NUS'" to generate $H^0 \rightarrow ee\nu\nu$-events, the datacard "WMODE2" was replaced with "WMODE2 'MU+', 'MU-'" to generate $H^0 \rightarrow \mu\mu\nu\nu$-events.

B.3 Super Symmetry.

```
SAMPLE SUPERSYMMETRY: SIMPLE DECAYS
40000, 10000, 0, 0/
SUPERSYM
JETTYPE1 'GL'/
JETTYPE2 'GL'/
GAUGINO  500, 5/
FORCE    29, 30, 1, -1/
PT        50,   20000,   50,   20000/
Y        -3.0,     3.0, -3.0,     3.0/
```